MOLECULAR CRYSTALS AND LIQUID CRYSTALS
2016, VOL. 630, 87–101
http://dx.doi.org/10.1080/15421406.2016.1146881

Taylor & Francis
Taylor & Francis Group

Synthesis of liquid crystals based on hydrogen-bonding of 4-(Octyloxy)benzoic acid with 4-alkylbenzoic acids

M. D. Miranda[a,b], F. Vaca Chávez[c], T.M.R. Maria[d], M. E. S. Eusébio[d], P.J. Sebastião[c], P. Martín-Ramos[b], J. L. Figueirinhas[c], and M. Ramos Silva[b]

[a]European Space Agency, Noordwijk, The Netherlands; [b]CFisUC, Department of Physics, University of Coimbra, Coimbra, Portugal; [c]Centre of Physics and Engineering of Advanced Materials, Physics Department, Instituto Superior Técnico, Universidade de Lisboa, Lisboa, Portugal; [d]CQC, Chemistry Department, University of Coimbra, Coimbra, Portugal

ABSTRACT

A molecular recognition process has been used to form new mesogenic molecular structures, where intermolecular hydrogen bonding occurs between 4-(octyloxy)benzoic acid (8BAO) and four 4-alkylbenzoic acids (nBAs, n = 2, 5, 6, 7). The synthesis of these complexes has been attained by resorting to mechanochemistry. The resulting materials have been characterized by polarizing optical thermal microscopy, differential scanning calorimetry, vibrational spectroscopy, X-ray powder diffraction, and ^{1}H NMR relaxometry. All the elements of the series show the formation of a mesophase. For one of the complexes, its electro-optical properties have also been assessed, resulting comparable to those of other widely used liquid crystals.

KEYWORDS

4-Alkylbenzoic acids; hydrogen bonding; liquid crystals; mechanochemistry; 4-(octyloxy)benzoic acid

1. Introduction

Liquid crystal (LC) phases exist in nature, for instance, the concentrated protein solution, which is extruded by a spider to generate silk, is in a LC phase [1], but man-manipulated molecules are actually the ones that have found applications in computer monitors, televisions, instrument panels, DVD players, gaming devices, watches, calculators, and telephones, just to name a few [2].

For the supramolecular chemist, there is great interest in studying LC systems, especially those in which the combination of supramolecular interactions and molecular shape may provide a mesophase [3, 4]. 4-(Octyloxy)benzoic acid (8BAO) is one of such substances. It melts into a smectic state at 101°C, with a transition to a nematic state at 108°C and finally to an isotropic state at 147°C [5]. In the crystalline form, the molecules assemble as centrosymmetric head-to-head H-bonded dimers, with the alkyl chains in an all-*trans* extended conformation. Overall, the molecules are neither linear nor planar, since the alkyl chain does not share the benzene ring mean plane [6].

The melting of a crystal begins in its loose aliphatic regions, progressively disordered, whereas the aromatic planar regions preserve their order at higher temperatures, thus

CONTACT M. Ramos Silva manuela@pollux.fis.uc.pt CFisUC, Department of Physics, University of Coimbra, Rua Larga P-3004 516 Coimbra, Portugal.

Color versions of one or more of the figures in the article can be found online at www.tandfonline.com/gmcl.

allowing the existence of a mesophase stabilized by intermolecular interactions. For the 4-alkyloxybenzoic acid series (*n*BAOs), there is a transition to a smectic phase followed by smectic-to-nematic and then to isotropic liquid. Conversely, the 4-alkylbenzoic series (*n*BAs) only show crystal-to-nematic and nematic-to-liquid transitions. It is thought that the difference in their behavior upon temperature increase is due to the existence of $\pi \ldots\pi$ interactions only in the alkyloxy series that are retained in the smectic phase. The alkyl series only show the H bonds as structure-forming elements (subsequently lost in the nematic phase). The length of the chain equally affects the two series: the longer the chain, the lower the melting temperature [7].

It is of interest to study the heteromolecular systems, where alkyloxybenzoic and alkylbenzoic molecules are mixed in a 1:1 proportion to investigate the effect of the supramolecular interactions. Madhu Mohan and coworkers have studied the 9BAO–12BAO alkoxy-alkyl series [8–11]. Here, we report the mechanosynthesis of the 8BAO + 2BA, 8BAO + 5BA, 8BAO + 6BA, and 8BAO + 7BA cocrystals and their thermal properties.

2. Experimental

2.1. Reagents and preparation method

4-(Octyloxy)benzoic acid (CAS No. 2493-84-7, 98%), 4-ethylbenzoic acid (CAS No. 619-64-7, 99%), 4-pentylbenzoic acid (CAS No. 26311-45-5, 99%), 4-hexylbenzoic acid (CAS No. 21643-38-9, 99%), and 4-heptylbenzoic acid (CAS No. 38350-87-7, 97%), shown in Figure 1, were supplied by Sigma-Aldrich (Sintra, Portugal).

The hydrogen-bonded complexes were obtained by a mechanosynthesis technique. The complexes were prepared by mixing 1:1 molar ratios of 4-(octyloxy)benzoic acid and one of the various 4-alkylbenzoic acids in a Retsch MM400 ball mill system (Retsch Solution in Milling & Sieving, Haan, Germany) with a 10 mL stainless steel grinding jar and two 7 mm diameter stainless steel balls per jar. A total mass of about 70 mg was used and mixing was performed for 1 h at 30 Hz. Each pure compound was also subjected to the same mechanical treatment. The resulting 8BAO + *n*BA cocrystals are white crystalline solids, stable at room temperature.

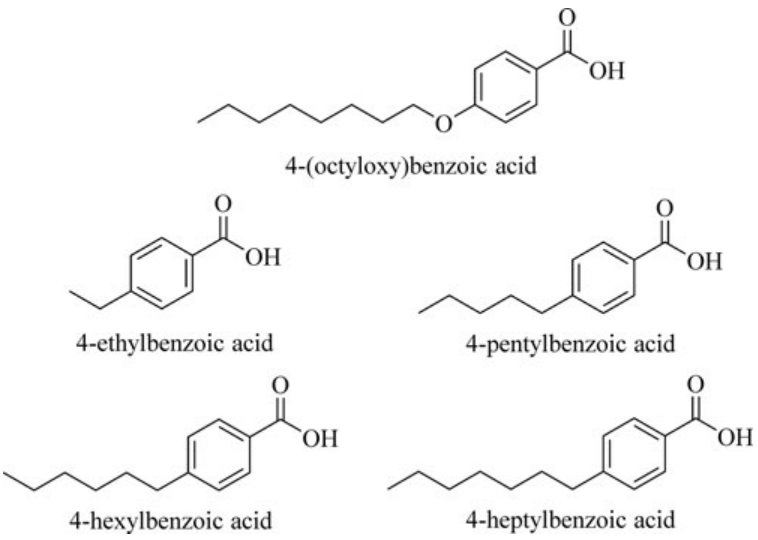

Figure 1. Chemical structures of 4-(octyloxy)benzoic acid (8BAO) and the 4-alkylbenzoic acids (*n*BAs, where $n = 2, 5, 6, 7$) under study.

2.2. Physical and optical measurements

X-ray powder diffraction (XRPD) experiments were conducted using an Enraf-Nonius powder diffractometer (Enraf-Nonius, Rotterdam, The Netherlands) equipped with a CPS120 detector (Inel, Artenay, France) and a quartz monochromator. Cu $K\alpha$ radiation was used ($\lambda = 1.540598$ Å). Silicon was utilized as an external calibrant.

Infrared spectra were recorded with a Thermo Nicolet 380 FT-IR apparatus (Thermo Scientific, Waltham, MA, USA) equipped with Smart Orbit Diamond ATR system.

Differential scanning calorimetry (DSC) data were obtained on a DSC Pyris1 Perkin Elmer calorimeter (Perkin-Elmer, Waltham, MA, USA), equipped with an intracooler cooling unit at −25°C (ethylene glycol–water, 1:1 v/v, cooling mixture), with a heating rate $\beta = 5$°C/min, under a N_2 purge, 20 mL/min. Samples were hermetically sealed in aluminum pans, and an empty pan was used as a reference. Temperature calibration was performed with high-grade standards, biphenyl (CRM LGC 2610, $T_{fus} = 68.93 \pm 0.03$°C), benzoic acid (CRM, LGC 2606, $T_{fus} = 122.35 \pm 0.02$°C), and indium (Perkin-Elmer, $x = 99.99\%$, $T_{fus} = 156.60$°C), which was also used for enthalpy calibration ($\Delta H_{fus} = 3286 \pm 13$ J·mol^{-1}) [12, 13].

Optical textural observations were made with a DSC600 hot/cold stage (Linkam Scientific Instruments Ltd., Guildford, Surrey, UK), equipped with a DMRB Leica microscope (Leica Microsystems, Wetzlar, Germany). Images of the samples, observed under polarized light and using wave compensator, were recorded using a Sony CCD-IRIS/RGB video camera at 200× magnification.

The proton spin-lattice relaxation time (T_1) was measured over a Larmor frequency (ν_L) range from 10 kHz to 300 MHz. Between 10 kHz and 8.9 MHz, the data were obtained with a custom-made fast field-cycling (FFC) spectrometer [14] operating with a polarization and detection field of 0.215 T and a switching time <3 msec. In the 10–91 MHz frequency range, a variable-field iron-core magnet equipped with a Bruker Avance II console was used. At 300 MHz, T_1 was measured with a Bruker Avance II spectrometer. Above 10 MHz, T_1 was measured applying the inversion recovery $(\pi)_x - \tau - (\pi/2)_{x,-x} - Acq$ sequence. For frequencies below 10 MHz, T_1 was measured using FFC NMR techniques (i.e., $B_P \rightarrow B_E - \tau - B_E \rightarrow B_D$) where the polarization field and detection fields, B_P and B_D, respectively, have the same value corresponding to the Larmor frequency of 8.9 MHz. Time τ was varied between zero and about five times the expected value of T_1 in order to decrease the uncertainty of the measured T_1.

The capacitance and birefringence data were measured by a computer-controlled system which comprised a HeNe laser ($\lambda = 0.6328$ μm) mounted on an optical bench and coupled to a signal generator and a voltage amplifier. The samples were placed in glass cells coated with indium-tin-oxide with a suitable treatment to induce a planar superficial alignment. Glass cells were purchased from INSTEC (Boulder, CO, USA). The thickness of the chamber, where the LC was stored, was 8.62 μm and was determined by interferometry. The sample temperature was kept constant (within 0.2°C) via a computer-controlled oven. The capacitance was determined by measuring both the AC voltage applied to the LC cell and the current flowing through the sample. In order to induce Freedericksz transitions, the amplitude of the AC voltage was changed at a certain rate, while the current and voltage were monitored with a TiePieHS4 oscilloscope (Sneek, Netherlands). The birefringence was determined by recording the intensities of the polarized parallel and perpendicular beams (relative to the linearly polarized incident beam) exiting the polarizing beam splitter, which received the laser light after orthogonally going through the cell with sample. These

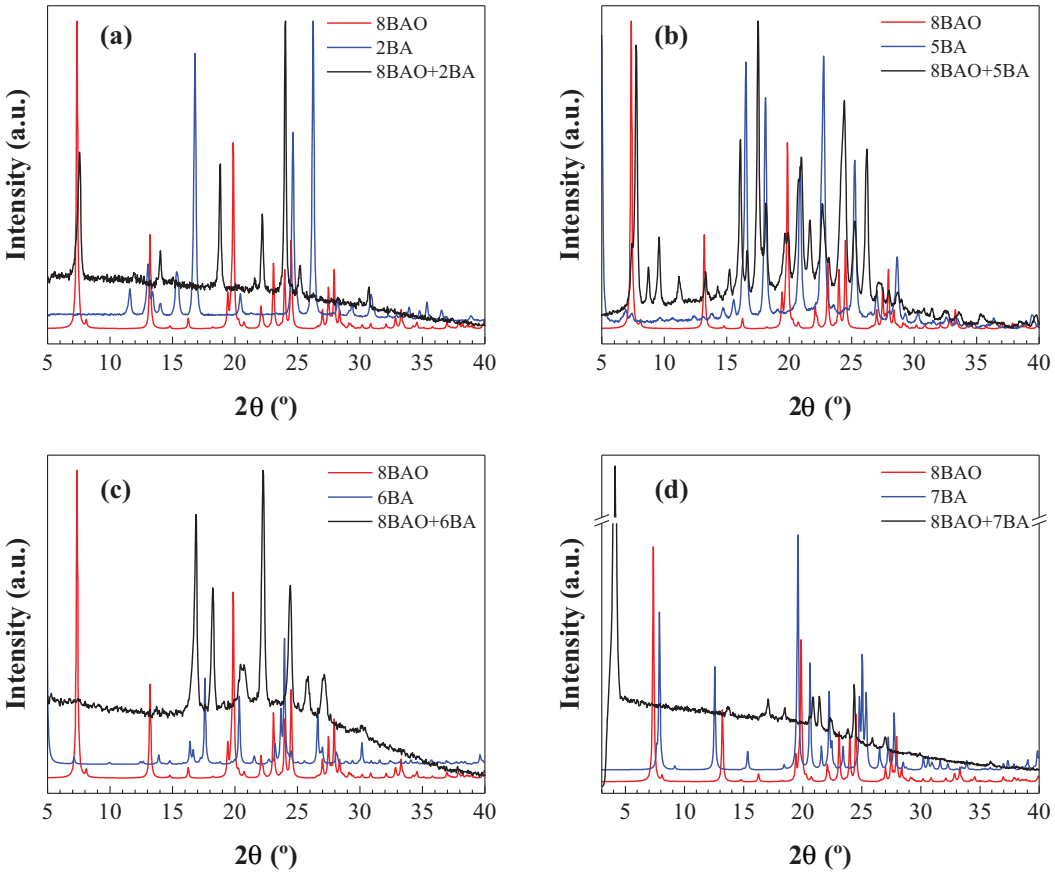

Figure 2. X-ray powder diffraction (XRPD) patterns for the cocrystals (black solid line) and for their individual constituents (red and blue solid lines): (a) 8BAO + 2BA; (b) 8BAO + 5BA; (c) 8BAO + 6BA; and (d) 8BAO + 7BA.

intensities were recorded using two other channels of aforementioned oscilloscope. The cell was placed perpendicularly to the incident laser beam with the polishing direction of the cell making a 45° angle with the direction of polarization of the linearly polarized incident beam.

3. Results and discussion

3.1. X-ray powder diffraction

X-ray powder diffraction (XRPD) was used to confirm the formation of new cocrystals by the mechanosynthesis technique. Figure 2 depicts the X-ray powder diffractograms for each of the 8BAO + *n*BA cocrystals, together with the diffraction patterns for their separate constituents. A visual inspection of the diffractograms shows that the cocrystals have molecular arrangements different from those of their corresponding individual components, with quite distinct peak positions and peak intensities. Furthermore, no significant residues of the single components are seen in the binary complex diffractograms, thus evidencing that all the starting materials have reacted.

3.2. Vibrational characterization

The infrared spectra of the hydrogen-bonded complexes 8BAO + *n*BA and their precursors are depicted in Figure 3.

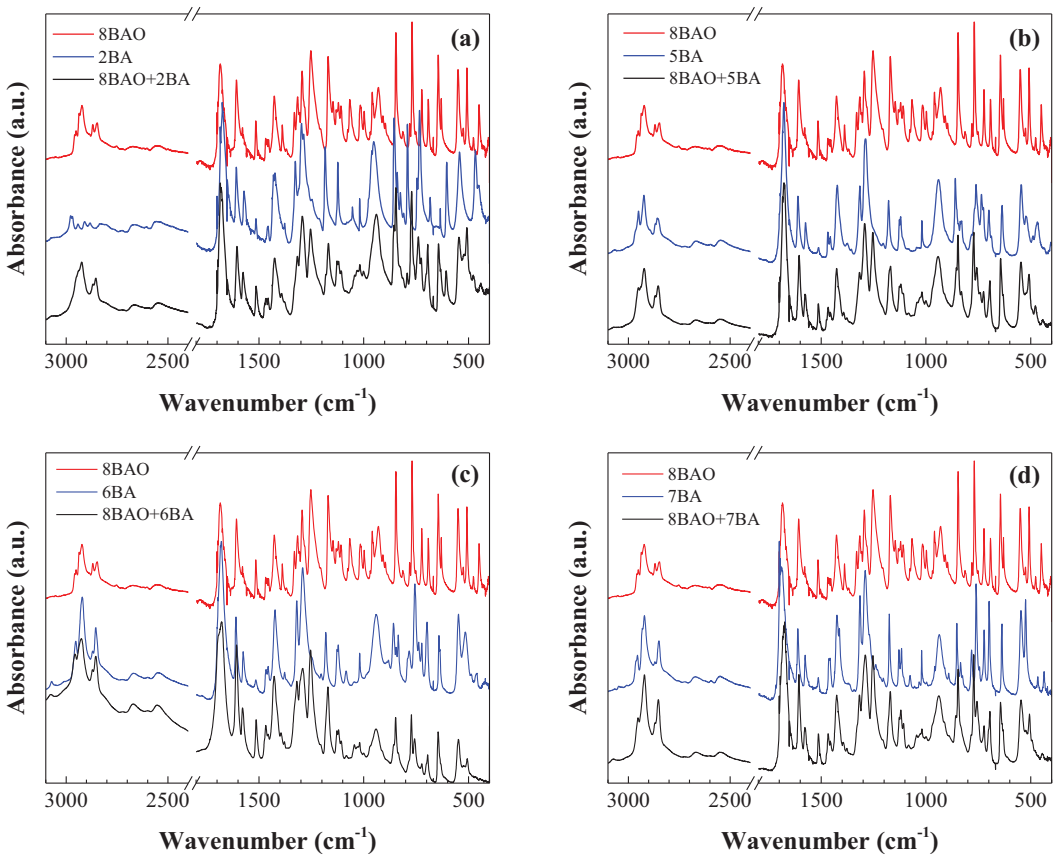

Figure 3. FTIR spectra of the four cocrystals (black solid lines) and of their corresponding individual constituents (red and blue solid lines): (a) 8BAO + 2BA; (b) 8BAO + 5BA; (c) 8BAO + 6BA; and (d) 8BAO + 7BA.

In the carboxylic acids, the characteristic frequencies for the O-H vibrations of the acidic group cover a wide region of the spectra, 3400–2400 cm^{-1}, centered at ~3000 cm^{-1}, due to hydrogen-bonding association between the acidic groups which gives rise to dimers [15, 16]. The C-H vibrations associated to the alkyl and aromatic groups also appear in the same region, overlapped with the former.

The C=O group vibrational frequency is typically observed in the 1730–1700 cm^{-1} region [16] for carboxylic acids associated as dimers. A shift to lower frequency is observed when compared to monomeric species (typically at 1760 cm^{-1}) [9, 17–19].

For the series of cocrystals under study, the heteroassociation is expected to occur, as for the pure components, by cyclic carboxylic acid hydrogen-bonded dimers. Therefore, only small differences are expected in the infrared spectra (see Table 1). For 8BAO + 2BA cocrystal, the absorption band attributable to C=O is observed at a wavenumber value between those of its individual components and the O-H band is centered at 2924 cm^{-1}, with a red shift of

Table 1. Characteristic IR absorption bands for the series of cocrystals and their precursors.

Cocrystals			Individual constituents		
8BAO + *n*BA	C=O (cm^{-1})	O-H (cm^{-1})	Precursor	C=O (cm^{-1})	O-H (cm^{-1})
8BAO + 2BA	1680	2924	2BA	1675	2978
8BAO + 5BA	1676	2922	5BA	1677	2924
8BAO + 6BA	1677	2925	6BA	1679	2921
8BAO + 7BA	1674	2921	7BA	1688	2921
			8BAO	1684	2922

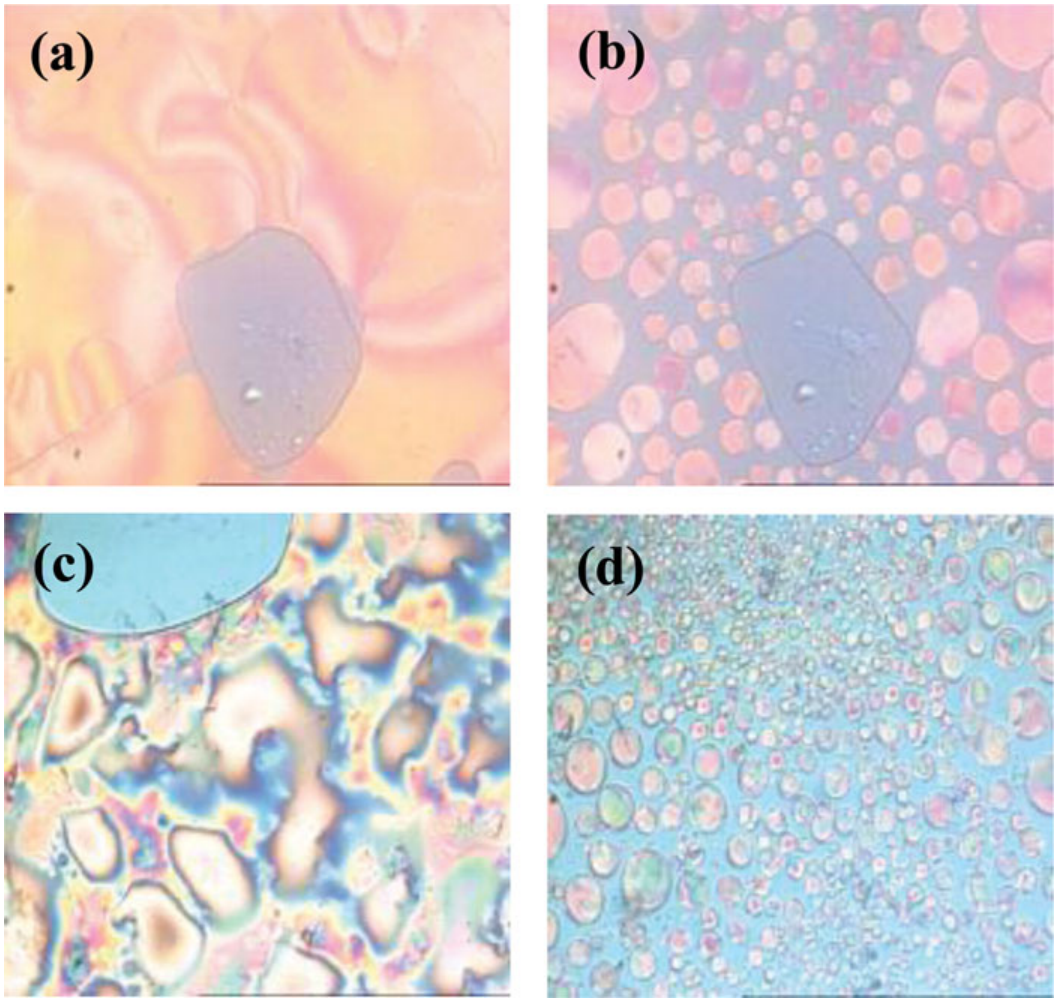

Figure 4. Texture of the *schlieren* nematic phase identified for two of the cocrystals during the heating/cooling cycles: (a) 8BAO + 2BA at 105°C, heating cycle; (b) 8BAO + 2BA at 121°C, cooling cycle; (c) 8BAO + 7BA at 132°C, heating cycle; and (d) 8BAO + 7BA at 130°C, cooling cycle. The polarized light microscopy measurements were conducted at a heating/cooling rate $|\beta| = 10$°C/min. Magnification: 200×.

about 50 cm^{-1} relatively to pure 2BA, indicative of a stronger hydrogen bond. For the intermediate members of the series, the differences for either bands cannot be regarded as significant. Nonetheless, the heteroassociation for the cocrystal with the largest 4-alkylbenzoic chain (8BAO + 7BA), results in a red shift of about 10 cm^{-1} for the C=O band when compared to those of its precursors (1674 cm^{-1} for 8BAO + 7BA cocrystal, instead of 1688 cm^{-1} for 7BA and 1684 cm^{-1} for 8BAO).

3.3. Thermal analysis and liquid-crystalline properties

The thermal behavior of the different 8BAO + *n*BA cocrystals was studied by DSC and complemented with polarized light microscopy measurements (see Figure 4), in order to identify –in addition to the transitions– the corresponding mesophases. The temperatures and enthalpies for the different phase transitions are summarized in Table 2.

The 8BAO + *n*BA cocrystals under study melted at temperatures below 72°C and showed a good thermal and chemical stability upon several heating/cooling cycles. For the cocrystals with 4-ethylbenzoic acid and 4-heptylbenzoic acid, the mesophase could be identified as a nematic one (Figure 4): upon cooling, in the transition from the isotropic phase to the mesophase, the *schlieren* nematic texture could be identified [9, 18, 20].

Table 2. Transition temperatures (°C) and enthalpies of transition (kJ/mol, in parenthesis) of the 8BAO + *n*BA cocrystals. T_{fus} = melting point, T_c = clearing point, and T_{cr} = crystallization point.

n	DSC cycle	T_{fus}	T_c	T_{cr}
2	Heating	69.6 (54.1)	126.9 (5.9)	
	Cooling		*N 125.1* (7.4)	59.6 (51.4)
5	Heating	54.0 (37.3)	133.2 (7.3)	
	Cooling		131.1 (6.9)	43.77 (35.3)
6	Heating	54.8 (28.5)	128.2 (4.7)	
	Cooling		125.7 (4.4)	49.9 (25.6)
7	Heating	72.0 (34.0)	132.6 (6.8)	
	Cooling		*N 132.9* (8.6)	68.4 (32.7)

The thermograms for the first heating cycle for all of the cocrystals are depicted in Figure 5. Two transitions could be identified in each case: in the first transition (from solid to mesophase) there is a gain of rotational and translational degrees of freedom, as in the nematic phase there is only global orientational order of molecules, while in the second transition this orientational order is lost, giving rise to an isotropic liquid. As expected [21], the first transitions involved energies >28.5 J g^{-1}, while the second transitions involved significantly lower energies (<7.3 J g^{-1}). These values are within the ranges reported in the literature for similar complexes [9, 17, 18, 22, 23].

Taking 8BAO + 7BA cocrystal as an example, a more detailed exam of its DSC curves can exemplify the behavior of the homologous series (see Figure 6): upon heating, the cocrystalwas thermally stable up to T_{fus} = 72.0°C (considering the onset value in the DSC curve), where there was a transition to a mesophase with ΔH_{fus} = 34.0 J·g^{-1}, corresponding to the first endotherm. The second transition (second endotherm), from the mesophase to the isotropic phase, occurred at T_c = 132.6°C with ΔH_c = 6.8 J·g^{-1} (as noted above, this enthalpy value was significantly smaller than that of the melting transition). In the cooling process, two exothermic effects were observed: the first one at T_{trs} = 132.9°C, with ΔH_{trs} = −8.6 J·g^{-1} (close in module to ΔH_c), would correspond to the formation of LC; the second exotherm, at T_{trs} = 68.4°C, with ΔH_{trs} = −32.7J·g^{-1} (close to the enthalpy value of the first transition in the heating cycle), would in turn correspond to the crystallization process.

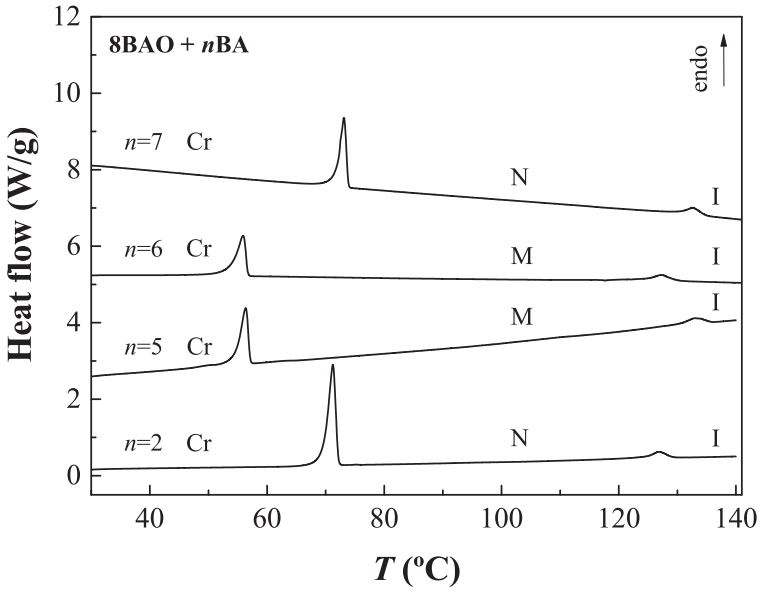

Figure 5. DSC heating curves for the different 8BAO + *n*BA cocrystals. β =5°C/min. Cr, N, M, and I stand for crystal phase, nematic phase, mesophase, and isotropic phase, respectively.

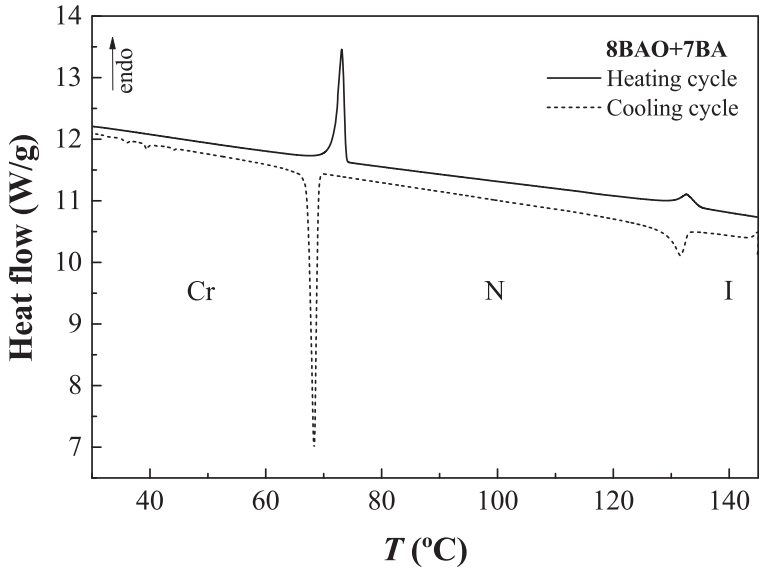

Figure 6. DSC first heating/cooling cycle for 8BAO + 7BA cocrystal (heating rate = 5°C/min and cooling rate = 10°C/min).

It is worth noting that the thermodynamic behavior of the cocrystal differs from that observed for each of its individual precursors [22, 23]. On the one hand, 4-(octyloxy)benzoic acid shows two distinct mesophases (a smectic one, with a transition at ~102°C, and a nematic one, with the transition at 109°C) followed by a transition to the isotropic phase at T_c = 149°C. On the other hand, 4-heptylbenzoic acid only shows a mesophase, which is nematic and occurs at 102°C, followed by the transition to the isotropic phase at T_c = 121°C.

A comparison of aforementioned values shows that the temperature at which the first transition took place for the cocrystal is much lower than those of its precursors. Moreover, the smectic phase present in pure 8BAO did not appear in the cocrystal.

With regard to the impact of the chain length of the 4-alkylbenzoic acids, Figure 7 shows a plot of the transition temperatures against the number of carbon atoms (n) in the alkyl chain.

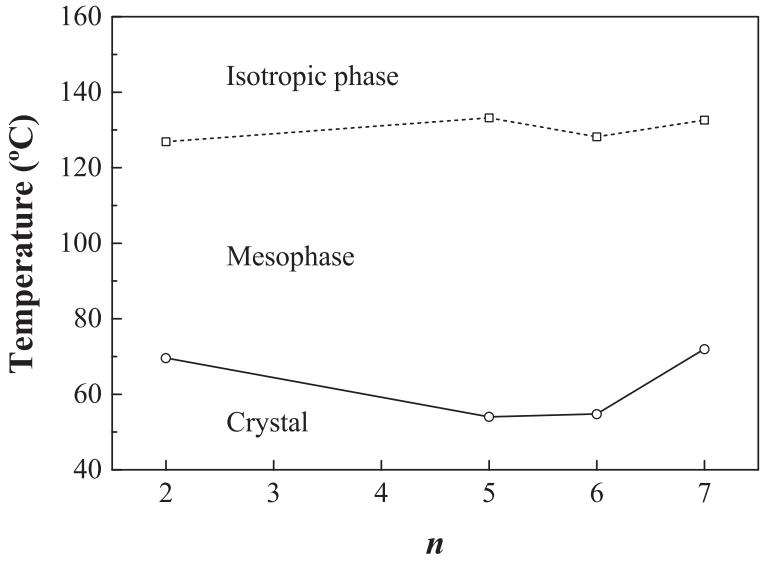

Figure 7. Plot of transition temperatures vs. number of carbon atoms (n) in the alkyl chain of the 4-alkylbenzoic acids for the series of 8BAO + nBA cocrystals.

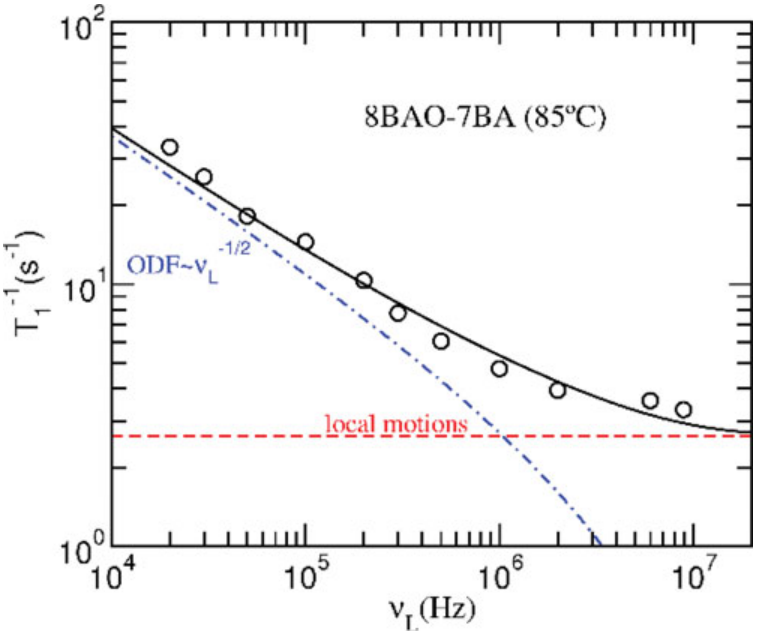

Figure 8. Fit of T_1^{-1} dispersion in the nematic phase at 85°C for the 8BAO + 7BA cocrystal. The solid line corresponds to the global fit. The dashed line (red) corresponds to the contribution of local rotations/reorientations and self-diffusion. The dot-dashed line (blue) corresponds to the collective motions with the typical $T_1^{-1} \sim \upsilon_L^{-1/2}$ dispersion.

3.4. Field-cycling NMR relaxometry measurements

The experimental spin-lattice relaxation rates are presented in Figure 8 as a function of the resonance frequency. In the studied frequency range, the experimental results are described by a sum of relaxation contributions that include collective and individual motions. In the nematic phase, the collective motions' relaxation mechanism is associated with order director fluctuations and is inversely proportional to the square-root of the resonance frequency, as it is typically observed for nematic phases of thermotropic LCs. In the high frequency regime (above 1 MHz), the relaxation contributions associated to individual motions are usually dominant.

3.5. Electro-optical measurements

In this section, we discuss the electro-optical parameters obtained for the 8BAO + 7BA cocrystal, and compare them with those of other well-known LCs, such as 4-cyano-4-*n*-pentylbiphenyl (5CB) so as to assess the performance of the former.

The capacitance and light transmittance ($I_{a2\perp}/I_{a1\parallel}$) curves as a function of the applied AC voltage at different temperatures, in the nematic phase, are depicted in Figure 9. At each temperature, the data were registered with a variable voltage at the maximum amplitude, starting from a low value, subsequently increasing it up to the maximum value considered and then returning to the starting value, allowing a long enough wait time to ensure that the obtained values corresponded to the stationary state of the directors. In a first analysis of the capacitance curves, it is possible to identify a soft landing for low voltage values, which increases with tension. This behavior occurs for all the analyzed temperatures and is the one expected for a uniaxial nematic crystal. In the planar cell where the sample is located, the director begins, for low voltage values, parallel to the sample surface and the capacity is given by $C = \varepsilon_\perp S/d$; for $\Delta V = \Delta V_c$ ($\Delta V_c = \pi\sqrt{K_{11}/(\varepsilon_\parallel - \varepsilon_\perp)}$), Freedericksz transition occurs and the capacitance

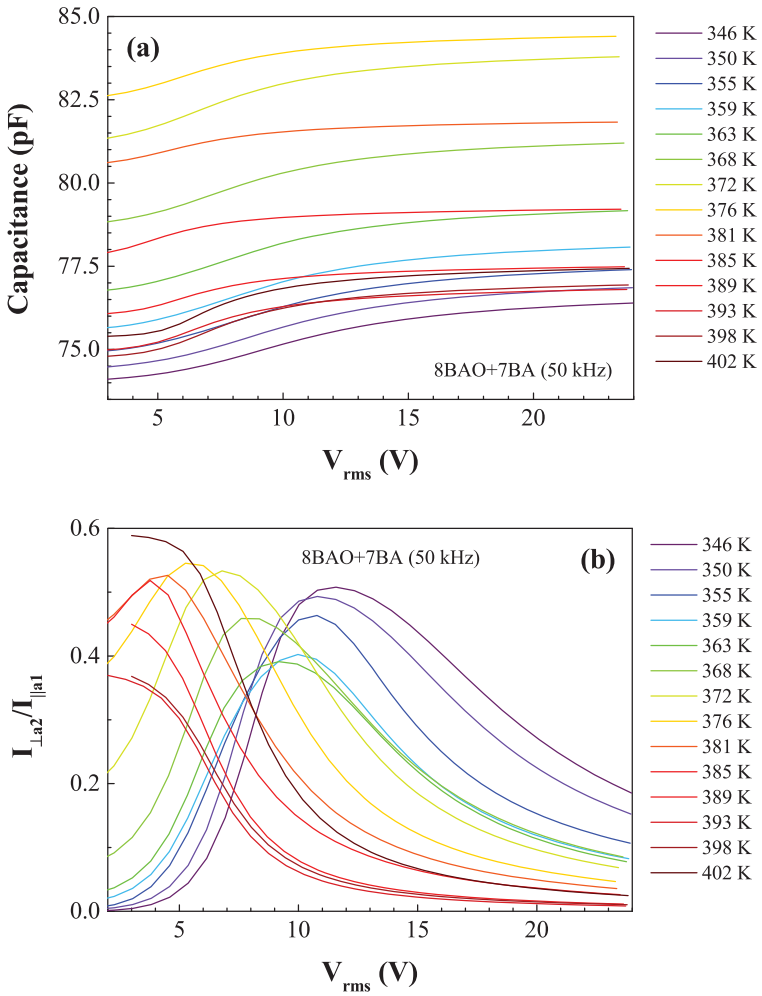

Figure 9. (a) Capacitance and (b) transmittance of 8BAO + 7BA cocrystal as a function of the applied voltage at different temperatures in the 346–402 K range. The AC frequency was 50 kHz in all cases.

begins to rise as ΔV increases and approaches the threshold $C = \varepsilon_{\parallel} S/d$. Figure 10 shows some of the capacitance and transmittance curves together with their respective theoretical fits.

The model used to fit both the voltage dependence of the capacitance and the light transmission is described in detail in ref. [24]. In this model, the director field is determined from the minimization of the appropriate free energy considered for the LC in the optical cell. It comprises both the Frank elastic free energy contribution and the electric field contribution [25]. From the director field in the sample, the electrical capacitance is calculated and, using a generalized Jones matrix formalism, one also obtains the transmission coefficient for the 90° rotated component of the light that has passed orthogonally through the optical cell [24]. The free energy density used in the model has the form:

$$F = \frac{1}{2}K_{11}\left(\nabla.\vec{n}\right)^2 + \frac{1}{2}K_{22}\left(\vec{n}.\nabla \times \vec{n}\right)^2 + \frac{1}{2}K_{33}\left(\vec{n} \times \nabla \times \vec{n}\right)^2 - \frac{1}{2}\varepsilon_{ij}E_iE_j$$

where K_{ii} are Frank elastic constants, ε_{ij} is the ij dielectric tensor component, and E_i is the ith component of the electric field. The electric field is not uniform in the nematic cell and is also determined in the minimization process, as detailed in ref. [24]. To simplify the analysis, the director is assumed to vary solely with the normal distance to the cell plates and is constrained to vary in the plane XOZ with the cell plates located at $z = \mp d/2$. The director

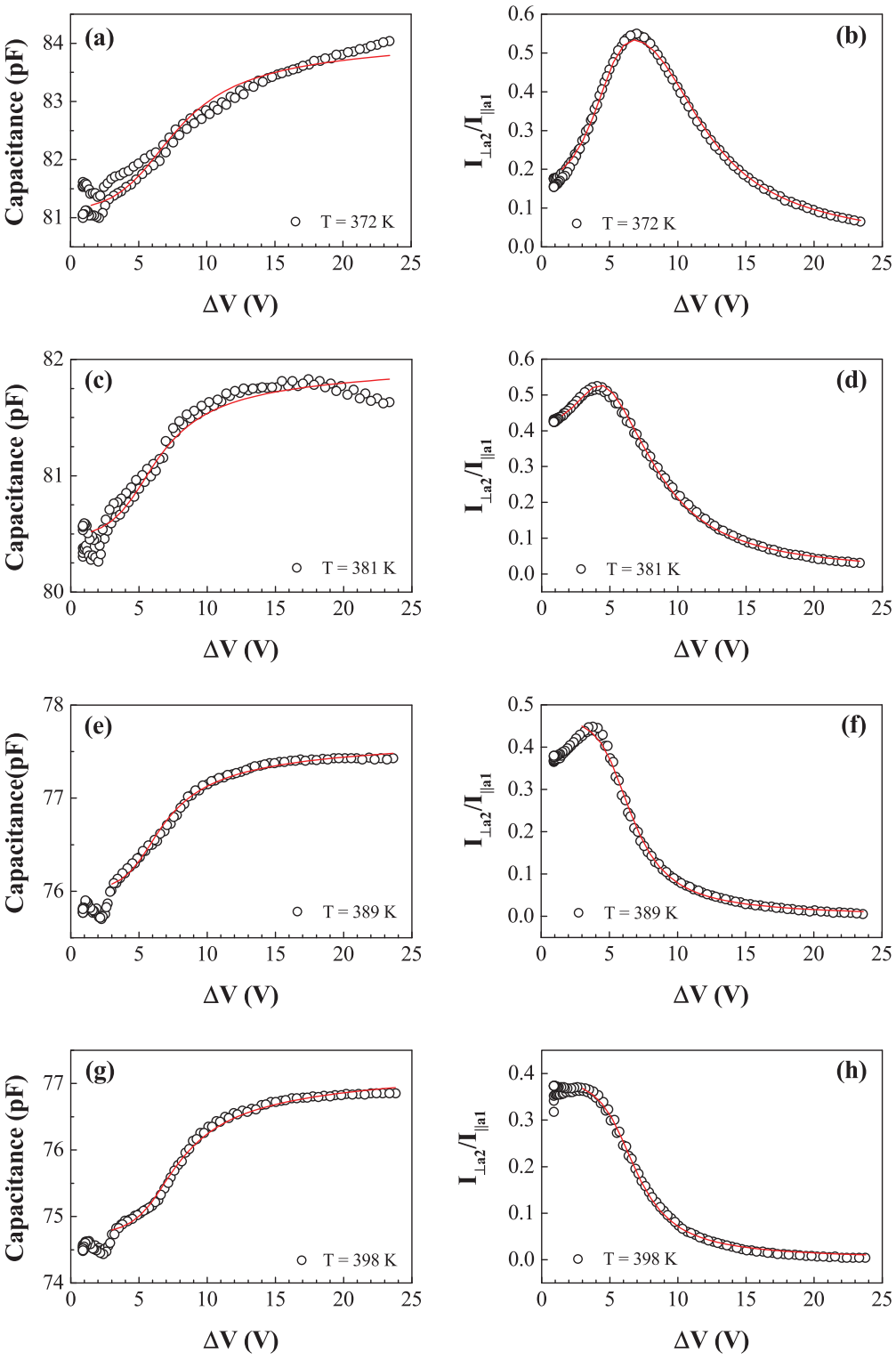

Figure 10. Dependence of capacitance (left column) and transmittance (right column) on the applied voltage, at four different temperatures, for 8BAO + 7BA cocrystal. The corresponding theoretical fits are shown as solid red lines. The AC frequency was 50 kHz in all cases.

is parameterized as $\vec{n} = \cos(\theta(z))\hat{e}_x + \sin(\theta(z))\hat{e}_z$. Under these considerations, the Euler–Lagrange equation for the director defining angle (z) is:

$$\left[K_{11}cos^2\theta + K_{33}sin^2\theta\right]\frac{d^2\theta}{dz^2} + \frac{1}{2}sin2\theta\left[K_{33} - K_{11}\right]\left(\frac{d\theta}{dz}\right)^2 + \frac{1}{2}sin2\theta\,\Delta\varepsilon\left\langle E^2\right\rangle = 0$$

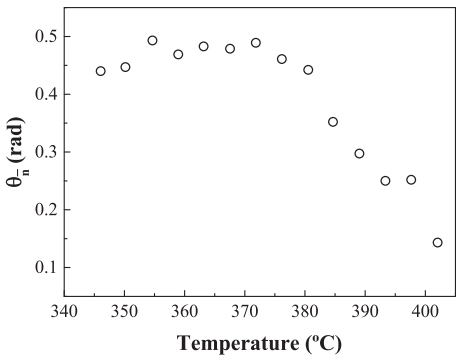

Figure 11. Dependence of the director ($\vec{n}$) tilt angle with temperature on the surface of the cell for the 8BAO + 7BA cocrystal.

where $\Delta\varepsilon$ is the dielectric anisotropy and $<E^2>$ is the RMS electric field squared. The capacitance is calculated from the relation:

$$C = \frac{Q}{\Delta V} = \frac{S}{\int_0^h \varepsilon_{zz}^{-1} dz},$$

where S is the area of the conductive surfaces of the cell and h is the LC cell thickness. Details can be found in ref. [24].

The fittings of the voltage dependence of the capacitance, partially shown in Figure 10, reveal the presence of a tilt of the director at the cell surfaces. Its temperature dependence is shown in Figure 11.

This tilt angle, $\theta_{\vec{n}}$, is nonzero and remains remarkably constant up to ~375 K. Above this temperature, it starts to decrease as the temperature is further increased. Although this angle should have been zero due to the surface treatment of the cell, the final value is actually determined by the interaction of the LC with the polymer film predeposited by the manufacturer on the cell surfaces. The nonzero angle may be due to a particular conformation of molecular aggregates formed in the complex. At low temperatures, this structure would become dominant, leading to the increase in $\theta_{\vec{n}}$ values.

Figure 12 illustrates the dependence of the dielectric constants $\varepsilon_\perp$ and $\varepsilon_\parallel$ with temperature, measured on the basis of the capacitance fits. The maximum variation detected for both $\varepsilon_\perp$ and $\varepsilon_\parallel$ in the temperature range analyzed is below 15%. It is also possible to identify two separate zones with different dependencies, below and above $T = 375$ K: in the former ($T < 375$ K), the dielectric constants increase with increasing temperature; while in the second region, they decrease as the temperature is further increased. This nonmonotonous and similar temperature dependence for both $\varepsilon_\perp$ and $\varepsilon_\parallel$ is unusual in common nematics (e.g., in 5CB, both dielectric constants vary monotonously but while $\varepsilon_\perp$ increases, $\varepsilon_\parallel$ decreases as the temperature is increased from 388 K to 408 K [26]). Nonetheless, the dielectric constants values are within the range of those typically found in nematics, though the dielectric anisotropy is rather small [24]. In fact, the observed behavior could be linked with the director surface tilt change discussed above, which gradually varies above 375 K. When only the data in the 345 and 375 K range is considered, a monotonous dependence is verified [26–28], albeit with an unexpected slope for $\varepsilon_\parallel$.

Figure 13 shows the dependence of the elastic constant K_m of the nematic phase of 8BAO + 7BA sample. Due to the quality of the data, it was not possible to separate K_{11} and K_{33} and $K_{33} = K_{11}$ had to be considered, so the K_m value is actually an average elastic constant associated with the deformation of the nematic crystal. Again, in connection with the misalignment of the director at the cell surface, the K_m data also suffer from an unexpected dependence

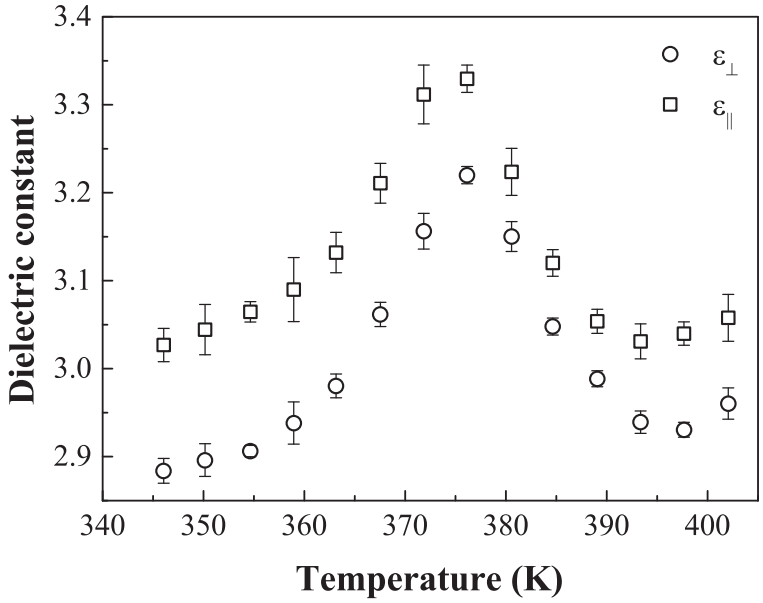

Figure 12. Dependence of the $\varepsilon_{\perp}$ and $\varepsilon_{\parallel}$ dielectric constants with temperature for 8BAO + 7BA, measured at an AC frequency of 50 kHz.

above 375 K. Nonetheless, if only the data in the 340–375 K is considered, the average elastic constant presents a dependence that would be perfectly normal for common nematic LCs and that would be comparable to the values obtained for 5CB [26]. The results discussed above for the dielectric constants $\varepsilon_{\perp}$ and $\varepsilon_{\parallel}$ and the average elastic constant K_m seem to indicate that around 380 K a change in the system is happening and this change may indicate an alteration in the molecular complexes.

The thermal dependence of birefringence is depicted in Figure 14, in which the birefringence was calculated from the n_e and n_o refractive indices. It is worth noting that the n_e and n_o refractive indices (not shown) showed significant fluctuations in their values, due to the fact that the chosen optical method is sensitive to $(n_e - n_o)$, but not to their separate values. The n_e and n_o indices were obtained from the transmittance fits and are given by the square

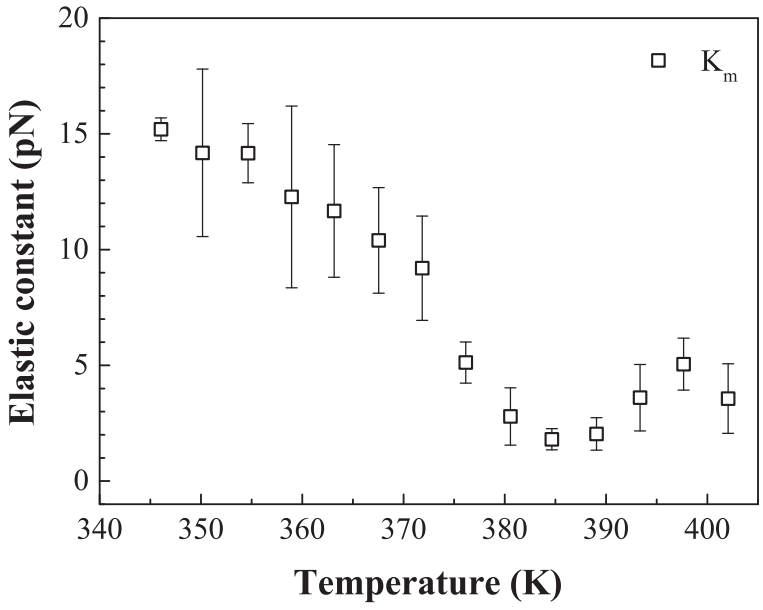

Figure 13. Dependence of the average elastic constant, K_m, with temperature for the 8BAO + 7BA cocrystal.

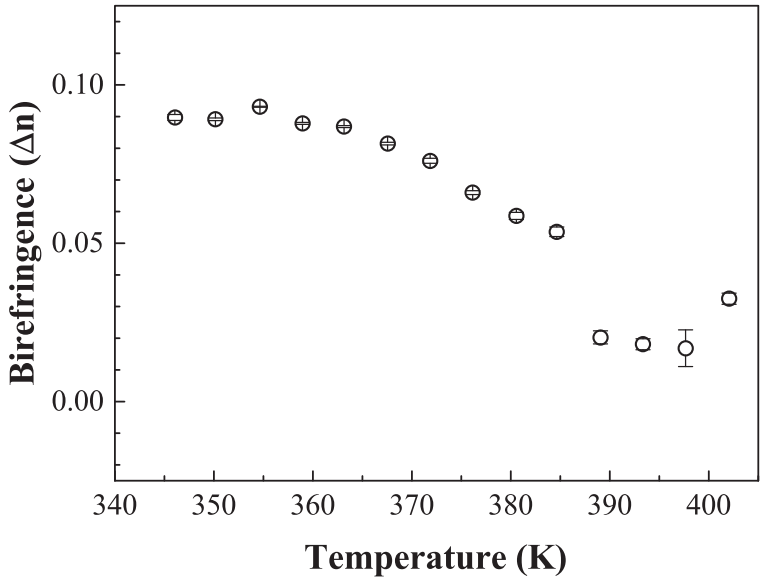

Figure 14. Dependence of the birefringence (Δn) with temperature for 8BAO + 7BA cocrystal.

root of the relative dielectric constants, $\varepsilon_{\perp}$ and $\varepsilon_{\parallel}$, but measured at the frequency of the laser source used $\upsilon = c/0.6328 \times 10^{-6}$ Hz, which is a very high frequency.

4. Conclusions

A new series of hydrogen-bonded LCs, formed by hydrogen bonding of 4-(octyloxy)benzoic acid (8BAO) and four different 4-alkylbenzoic acids (*n*BAs, where *n*=2, 5, 6, 7), has been obtained by a solvent-free approach, resorting to a mechanochemistry synthesis technique. The formation of the new complexes has been confirmed by XRPD and vibrational characterization.

The thermal behavior of the materials (studied by DSC and polarized light thermal microscopy (PLTM)) shows the presence of only one mesophase in all cases, which could be confirmed as a nematic mesophase for some of the complexes. Field-cycling NMR relaxometry measurements, conducted for one of those complexes, provide additional evidence of the fact that the relaxation mechanisms correspond to such phase, in agreement with PLTM results. The thermal behavior of the reported series 8BAO + *n*BA differs quite dramatically from the 9BAO + *n*BA series, where several smectic phases were identified. To fully understand the difference in the supramolecular interactions in such cocrystals, knowledge of the crystal structure in the solid phase is needed and crystallization of a single crystal is under way.

For one of the complexes, 8BAO + 7BA, electro-optical measurements have also been conducted, determining its birefringence and dielectric and elastic constants, which are comparable to those of the commonly used 4-cyano-4'-pentylbiphenyl (5CB).

Acknowledgments

F. Vaca Chávez, P.J. Sebastião, and J.L.M. Figueirinhas thank Portuguese Fundação para a Ciência e a Tecnologia (FCT) projects PEst-OE/FIS/UI0261/2011 and PEst-OE/FIS/UI0261/2014 for financial support. CQC is supported by FCT-Pest-OE/UID/QUI/00313/2013.

References

[1] Knight, D., & Vollrath, F. (1999). *Tissue and Cell*, *31*, 617.
[2] Tkachenko, G. V. (2009). *New Developments in Liquid Crystals*, In-Tech: Vienna, Austria.
[3] Paleos, C. M., & Tsiourvas, D. (2001). *Liq. Cryst.*, *28*, 1127.
[4] Miranda, M. D., Chávez, F. V., Maria, T. M. R., Eusebio, M. E. S., Sebastião, P. J., & Silva, M. R. (2014). *Liq. Cryst.*, *41*, 1743.
[5] Lokanath, N. K., Revannasiddaiah, D., Sridhar, M. A., & Prasad, J. S. (2000). *Mol. Cryst. Liq. Cryst. 348*, 7.
[6] Bryan, R. F., Hartley, P., Miller, R. W., & Shen, M.-S. (2007). *Mol. Cryst. Liq. Cryst.*, *62*, 281.
[7] Kuz'mina, L. G., Pestov, S. M., Kochetov, A. N., Churakov, A. V., & Lermontova, E. K. (2010). *Crystallogr. Rep.*, *55*, 786.
[8] Kavitha, C., Prabu, N. P. S., & Madhu Mohan, M. L. N. (2013). *Mol. Cryst. Liq. Cryst.*, *574*, 96.
[9] Kavitha, C., & Madhu Mohan, M. L. N. (2012). *J. Phys. Chem. Solids*, *73*, 1203.
[10] Kavitha, C., Prabu, N. P. S., & Mohan, M. L. N. M. (2012). *Phase Transitions*, *85*, 973.
[11] Kavitha, C., Pongali Sathya Prabu, N., & Madhu Mohan, M. L. N. (2012). *Physica B*, *407*, 859.
[12] Sabbah, R., Xu-wu, A., Chickos, J. S., Leitão, M. L. P., Roux, M. V., & Torres, L. A. (1999). *Thermochim. Acta*, *331*, 93.
[13] Della Gatta, G., Richardson, M. J., Sarge, S. M., & Stølen, S. (2006). *Pure Appl. Chem.*, *78*, 1455–1476.
[14] Mesquita Sousa, D., Domingos Marques, G., Manuel Cascais, J., & José Sebastião, P. (2010). *Solid State Nucl. Magn. Reson.*, *38*, 36.
[15] Kato, T., Kato, T., Fréchet, J. M. J., Uryu, T., Kaneuchi, F., Jin, C., & Fréchet, J. M. J. (2011). *Liq. Cryst.*, *33*, 1429.
[16] Pavia, D. L., Lampman, G. M., & Kriz, G. S. (2014). *Introduction to Spectroscopy*, Cengage Learning: Boston, MA.
[17] Prabu, N. P. S., & Mohan, M. L. N. M. (2012). *Mol. Cryst. Liq. Cryst.*, *569*, 72.
[18] Sathya Prabu, N. P., & Madhu Mohan, M. L. N. (2012). *J. Therm. Anal. Calorim.*, *113*, 811.
[19] Xu, J., Liu, X., Ng, J. K.-P., Lin, T., & He, C. (2006). *J. Mater. Chem.*, *16*, 3540.
[20] Prabu, N. P. S., Vijayakumar, V. N., & Madhu Mohan, M. L. N. (2012). *Phase Transitions*, *85*, 149.
[21] Goodby, J. W., Collings, P. J., Kato, T., Tschierske, C., Gleeson, H., & Raynes, P. (2014). *Handbook of Liquid Crystals*, Wiley-VCH Verlag GmbH: Weinheim.
[22] Monte, M. J. S., Almeida, A. R. R. P., & Ribeiro da Silva, M. A. V. (2004). *J. Chem. Thermodyn.*, *36*, 385.
[23] Fonseca, J. M. S., Santos, L. s. M. N. B. F., & Monte, M. J. S. (2010). *J. Chem. Eng. Data*, *55*, 2238.
[24] Polineni, S., Figueirinhas, J. L., Cruz, C., Wilson, D. A., & Mehl, G. H. (2013). *J. Chem. Phys.*, *138*, 124904.
[25] de Gennes, P. G., & Prost, J. (1995). *The Physics of Liquid Crystals*, Oxford University Press: Oxford.
[26] Bogi, A., & Faetti, S. (2001). *Liq. Cryst.*, *28*, 729.
[27] Collings, P. J., & Hird, M. (1997). *Introduction to Liquid Crystals Chemistry and Physics*, Taylor & Francis: London, Bristol, PA.
[28] Kato, T., Frechet, J. M. J., Wilson, P. G., Saito, T., Uryu, T., Fujishima, A., Jin, C., & Kaneuchi, F. (1993). *Chem. Mater.*, *5*, 1094.